Hindawi
International Journal of Chemical Engineering
Volume 2022, Article ID 9957189, 16 pages
https://doi.org/10.1155/2022/9957189

Research Article

Finite-Element Simulation of Electroosmotic Mixing: A Study of the Simultaneous Effects of Working Parameters for Optimization

Reza Kalantar Feeoj,[1] **Sayed Masoud Alavi Eshkaftaki**,[1] **Iman Kazemi Asfeh**,[1] **and Mehdi Jahangiri**[2]

[1]*Department of Mechanical Engineering, Shahrekord University, Shahrekord, Iran*
[2]*Energy Research Center, Shahrekord Branch, Islamic Azad University, Shahrekord, Iran*

Correspondence should be addressed to Mehdi Jahangiri; jahangiri.m@iaushk.ac.ir

Received 25 July 2022; Accepted 21 September 2022; Published 19 October 2022

Academic Editor: Maciej Jaskulski

Copyright © 2022 Reza Kalantar Feeoj et al. This is an open access article distributed under the Creative Commons Attribution License, which permits unrestricted use, distribution, and reproduction in any medium, provided the original work is properly cited.

Micromixers are crucial parts of microfluidic systems when it comes to efficiency and precision, as mixing is the central process in most relevant applications, including medical diagnosis, chemical production, and drug discovery. In view of the importance of improving the mixing quality, for the first time, the present work investigates the simultaneous effects of mixing chamber geometry (circular, hexagonal, and octagonal), electric field frequency (5, 7, 10, and 15 Hz), inlet velocity (0.1-0.2 $mm{\cdot}s^{-1}$), and phase difference (0-π) on the flow inside an electroosmotic micromixer using the finite-element tool COMSOL Multiphysics 5.4 to optimize the process and achieve homogeneous mixing. The flow-field, concentration-field, and electric-field equations were coupled and solved simultaneously. The results of this research indicated that at a given inlet velocity and a specific frequency range, as frequency increases, more mixing occurs in a smaller chamber, and as the inlet velocity increases, more mixing occurs in a smaller chamber at a higher frequency. Moreover, the highest mixing level (98.16%) was obtained with a 0.1 $mm{\cdot}s^{-1}$ inlet velocity, 10 Hz frequency, and $\pi/2$ phase difference in a hexagonal chamber.

1. Introduction

Mixing is a vital process in the chemical and pharmaceutical industries. Further, mixing by microfluidic systems has been a favorite topic in recent decades [1]. Micromixers are notable microfluidic systems that serve to mix two or more phases. Accordingly, these systems have received considerable attention from the research community.

Based on different mixing mechanisms, micromixers are classified into two types of active and passive [2]. A passive micromixer is the one in which mixing percentage is increased by deforming the micromixer geometry [3]. In active micromixers, external forces such as electric force and magnetic force are used to make mixtures [4, 5]. An example of active micromixers is electroosmotic micromixer by which a considerable mixing percentage can be achieved [6]. To clarify the electroosmotic flow, it should be mentioned that electro-osmosis is a phenomenon in which the electric force applied on the net charge of the electric double layer is created by an external electric field, moving the electric charges. Therefore, fluid viscosity causes the fluid to move at sections farther than the electric double layer and the channel center, and ultimately, the fluid keeps moving throughout the microchannel [7].

Additionally, there are generally two important considerations in micromixers: one is short mixing time (the fluid achieves the highest mixing percentage in a shorter time), and the second one is shortening the microchannel, thereby saving costs to a considerable extent. Channels of passive micromixers are typically long with a complicated geometry, prolonging the time to achieve higher mixing percentages [8]. Therefore, using an external force such as an

Table 1: Values of used variables in this simulation.

Parameter	Value	Unit
ρ	10^3	kg/m^3
μ	10^{-3}	Pa.s
ε_r	80.2	—
σ	0.11845	S/m
ζ	−0.1	V
V_0	0.1	V
D	10^{-11}	m^2/s
c_0	1	mol/m^3

electric force exerted on the fluid by electrodes can, to some extent, decrease the mixing time and the microchannel length, yet achieving a higher mixing percentage in a shorter time [9].

In electroosmotic micromixers, electrodes are the main cause of fluid eddies and the consequent increase in mixing percentage. Factors affecting electrode-induced eddy include electrode length, type of arrangement, and number of electrodes [10–13].

In AC electroosmotic micromixers, arrangement of electrodes is of much importance. For instance, a face-to-face arrangement gives more mixing than a pair of planar electrodes [14].

Another factor affecting mixing percentage in electroosmotic micromixers is phase and frequency differences [15–17].

Augmenting the electric current can also lead to creating eddies and increasing mixing percentages [18]. However, it should be noted that higher mixing percentage is not achieved merely by augmenting the electric current [19].

One of the factors, having a great effect on increasing mixing percentage in micromixers, is geometrical changes and the presence of obstacles along the fluid path, which was examined in active micromixers [20]. Compared to T-shaped micromixers, geometrical changes of the mixing chamber and the presence of obstacles with different shapes would yield much better results [21].

As stated previously, the shorter the length of the fluid microchannel, the higher the economic feasibility of fabricating this micromixer. In this regard, increasing the flow velocity will decrease the fluid inertia and the mixing percentage [22]. It can be clearly understood that by increasing the flow velocity, a longer channel would be needed to conduct better mixing [23].

Upon reviewing the literature, this question was posed that whether there is any logical relationship between parameters such as flow velocity, frequency, phase difference, and mixing chamber geometry in order to achieve a higher mixing percentage.

Though totally invaluable, none of these studies examined the close relationship between the abovementioned parameters and the mixing chamber geometry. The present research investigated, for the first time, the simultaneous effect of these parameters in micromixers and a mixing chamber symmetric about the x-axis. It was observed that at a specific velocity and phase difference, a mixing chamber with the smallest area at frequencies higher than the specific frequency range and a mixing chamber with the biggest area at frequencies lower than the specific frequency range have better efficiencies in achieving a higher mixing percentage.

2. Present Work

This research examined three 2-dimensional electroosmotic micromixers with symmetric circular, octagonal, and hexagonal mixing chambers at 3 different velocities and 3 phase differences in COMSOL 5.4 finite-element analysis software.

The mixing quality was calculated with each configuration in the simulations by adjusting inlet velocity, frequency, and phase difference. Moreover, the simultaneous and mutual effects of these factors on the mixing quality were discussed to determine the optimal mixing conditions. Different inlet velocities ($0.1 \le u \le 0.2$ mm·s^{-1}), phase differences ($0 \le \varphi \le \pi$ rad), and frequencies ($5 \le f \le 15$ Hz) were examined. Table 1 lists the simulation parameters. The following geometries were used in each micromixer (Figures 1(a)-1(c)). Further, details of segment A (Figure 1(d)) are presented, showing the mixing chamber inlet size.

3. Governing Equations

The present section begins by going through the governing equations of the electroosmotic flow of a Newtonian fluid inside a micromixer under incompressible and steady conditions. Then, the equations governing the concentration of species are presented to investigate mixing and calculate the efficiency.

3.1. Flow Field. The flow was studied using the time-dependent Navier–Stokes equation for two-dimensional flow. Continuity and Navier–Stokes equations of the problem are as follows:

$$\begin{aligned} \nabla.u &= 0, \\ \rho \frac{Du}{Dt} &= -\nabla p + \mu \nabla^2 u + F, \end{aligned} \tag{1}$$

where u represents velocity (m.s^{-1}), ρ shows fluid density (kg.m^{-3}), μ denotes the dynamic fluid viscosity (kg.m^{-1}.s^{-1}), and p and F are the pressure (Pa) and the electrokinetic force (N.m^{-3}), respectively.

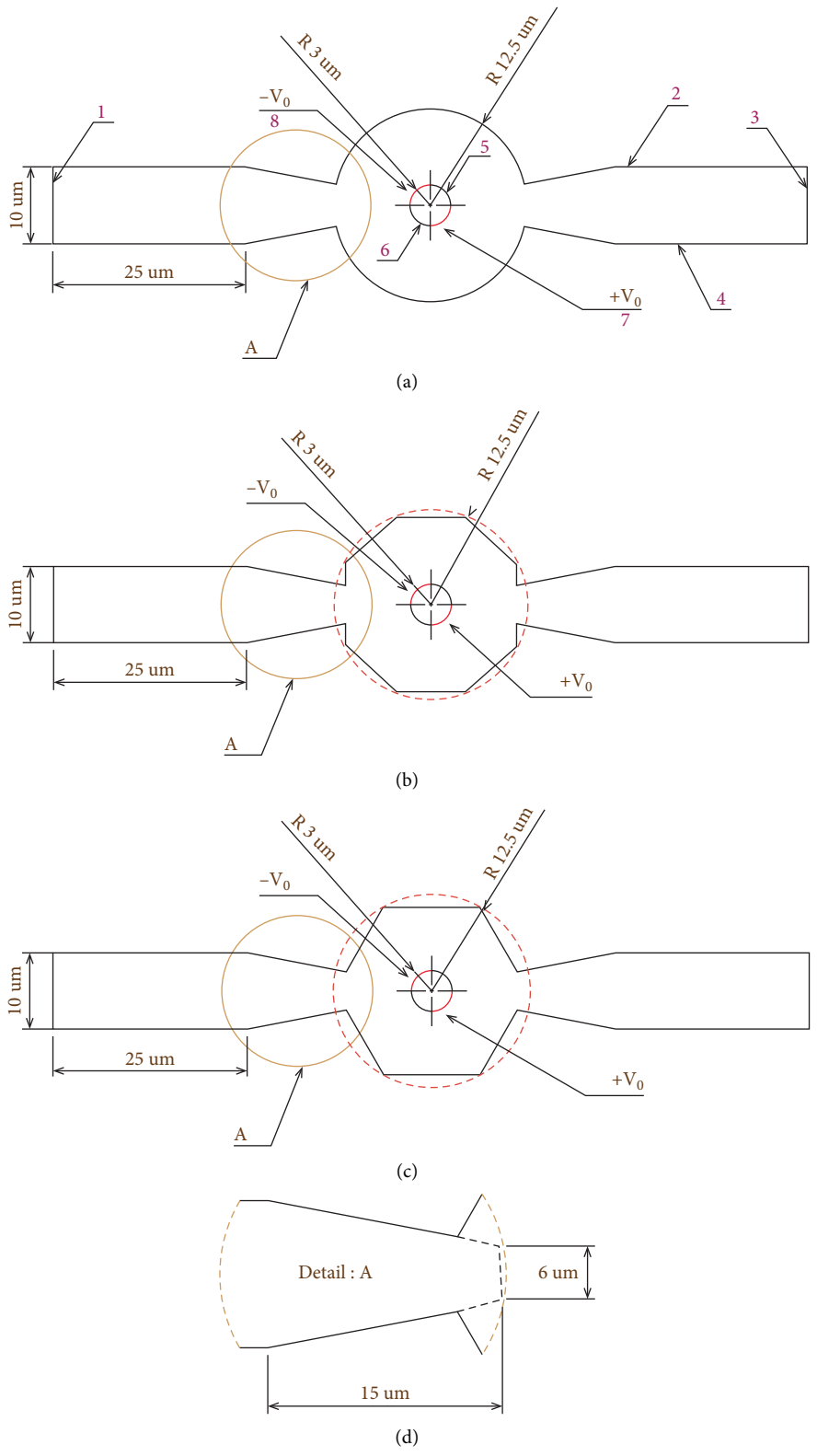

Figure 1: Geometries studied in the present work: (a) circular; (b) octagonal; (c) hexagonal (d) detail A.

Table 2: Different solutions to test grid independence.

Case no.	1	2	3	4	5	6
No. of elements	3703	5057	9022	14407	18076	24916

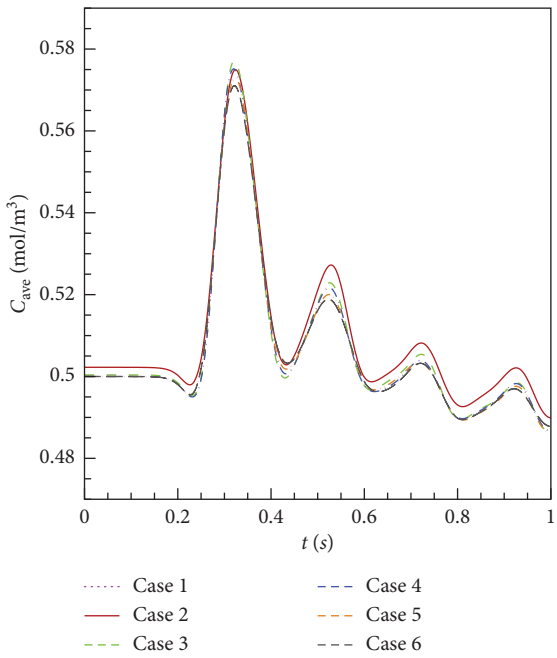

Figure 2: Changes in concentration with time plotted to test the solution's grid independence.

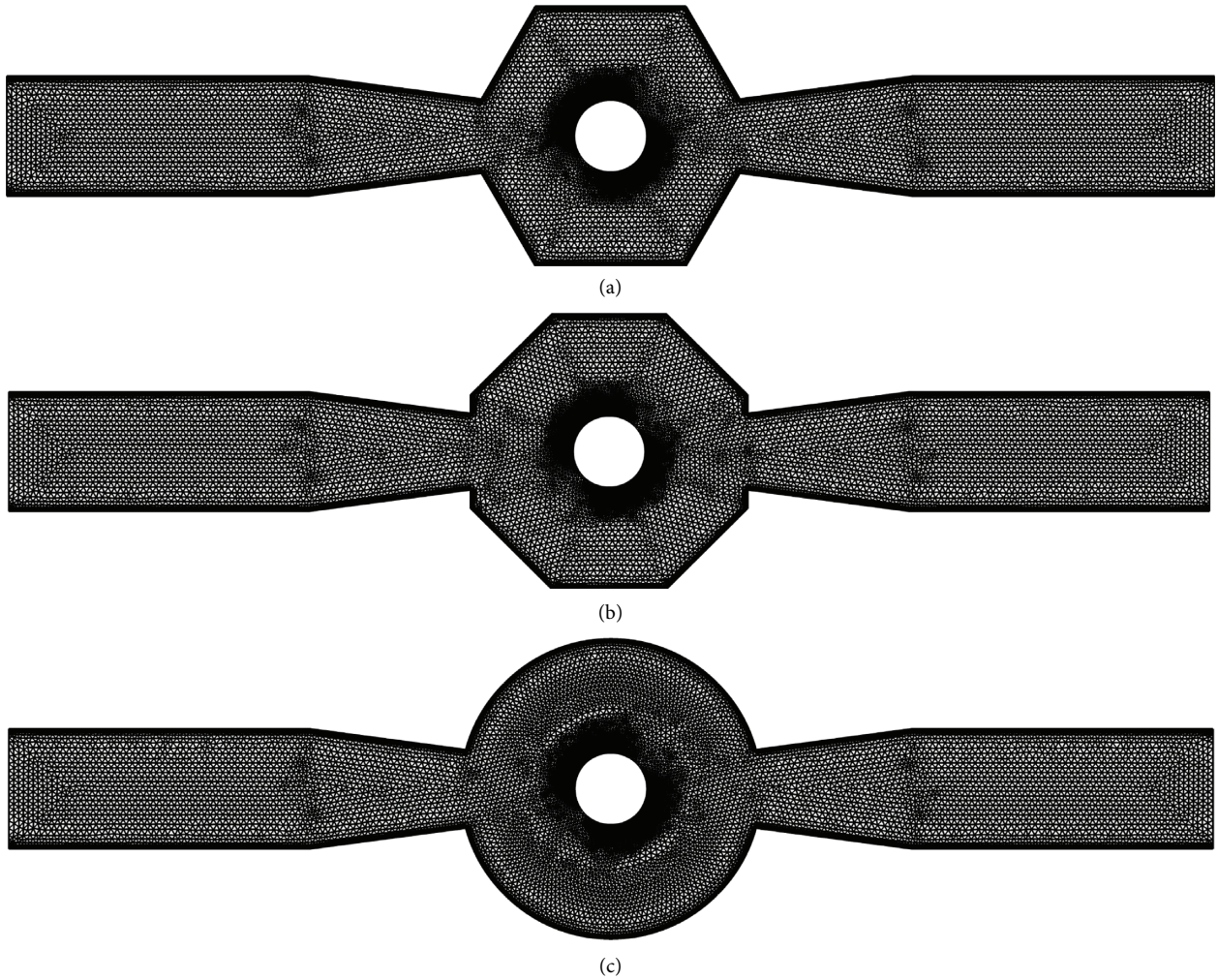

Figure 3: Meshing of micromixer mixing chambers: (a) hexagonal; (b) octagonal; and (c) circular.

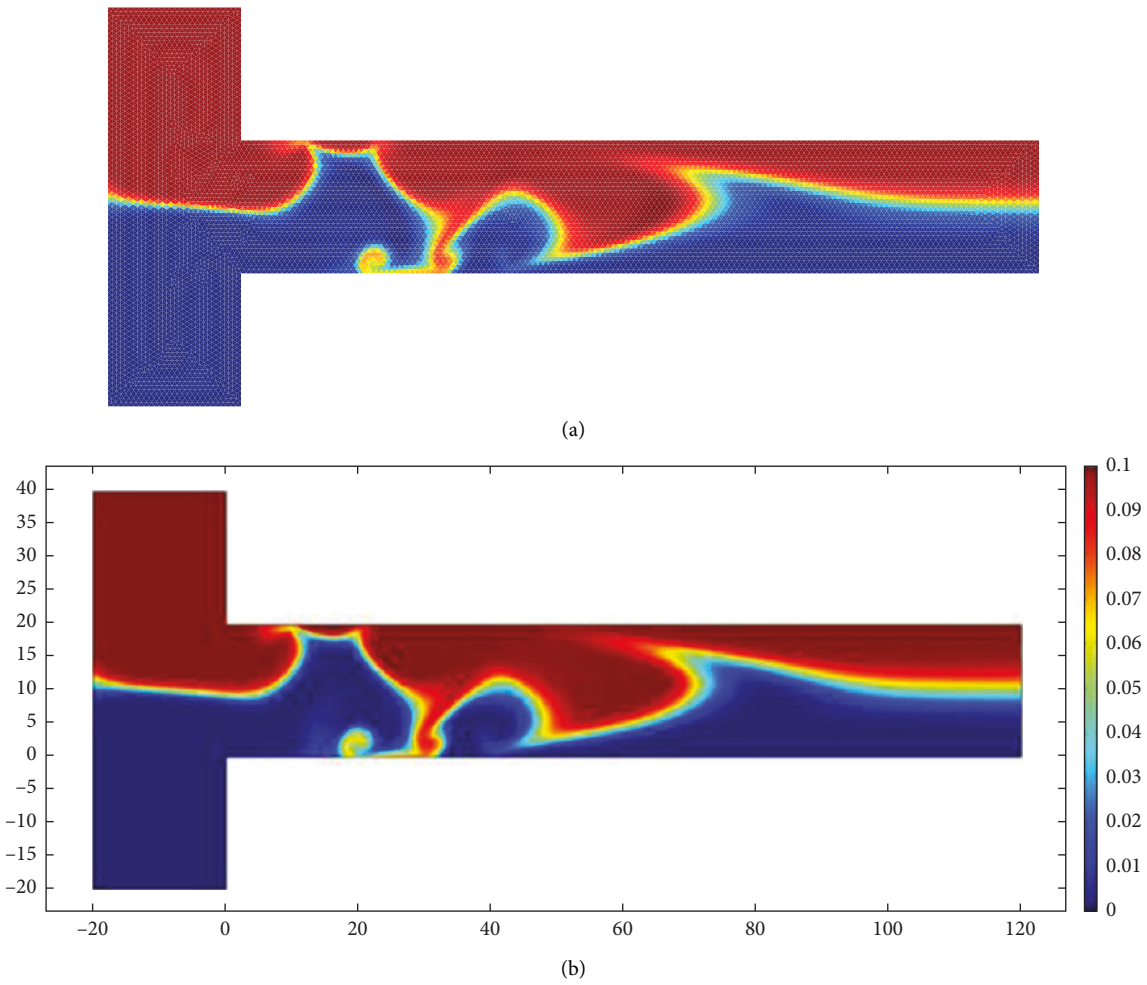

Figure 4: Concentration contours under sinusoidal potential at 100 Hz and $t = 0.02/3$ s in the (a) present study and (b) Cheng et al. [22].

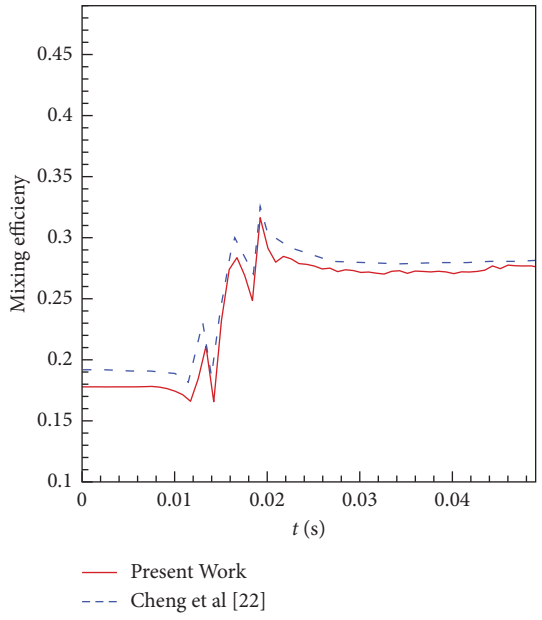

Figure 5: Comparison between mixing efficiency of present work and Cheng et al. [22] at $f = 400$ Hz with sine wave.

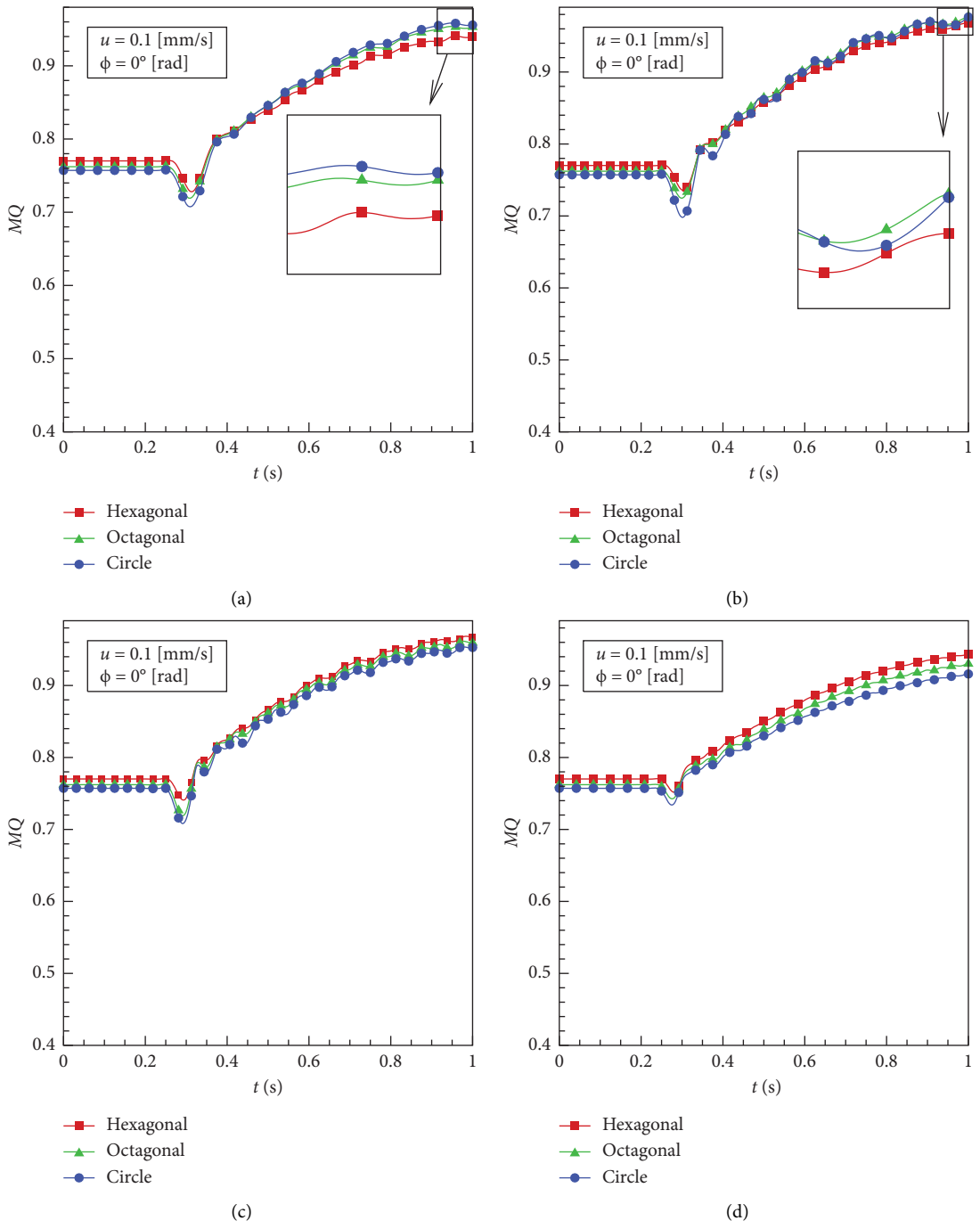

FIGURE 6: Mixing efficiency variation based on time in three mixing chambers at $u = 0.1$ mm·s^{-1} and $\varphi = 0$ for different frequencies: (a) 5 Hz; (b) 7 Hz; (c) 10 Hz; and (d) 15 Hz.

In this research, from Figure 1 it can be seen that the fluid entered the microchannel via Boundary No. 1, crossed over the mixing chamber, and exited from Boundary No. 3. At the inlet, flow was fully developed and slow. In all walls, the boundary condition of electroosmotic velocity was established, and at the outlet, pressure was equal to the atmospheric pressure.

The electric double layer has a zeta potential of $\zeta(V)$, and the thickness of the electric double layer is referred to as the Debye length. The thickness is 0.1 nm and can be ignored when the microchannel width is more than 100 times as large as the Debye length [22]. All effects of electric charges and the electric field can be modeled by a single slip velocity boundary condition from the Helmholtz–Skolimowski equation [24]:

$$E = -\nabla V,$$
$$u_E = -\frac{\varepsilon E}{\mu}\zeta = \frac{\varepsilon\zeta}{\mu}\nabla V, \tag{2}$$

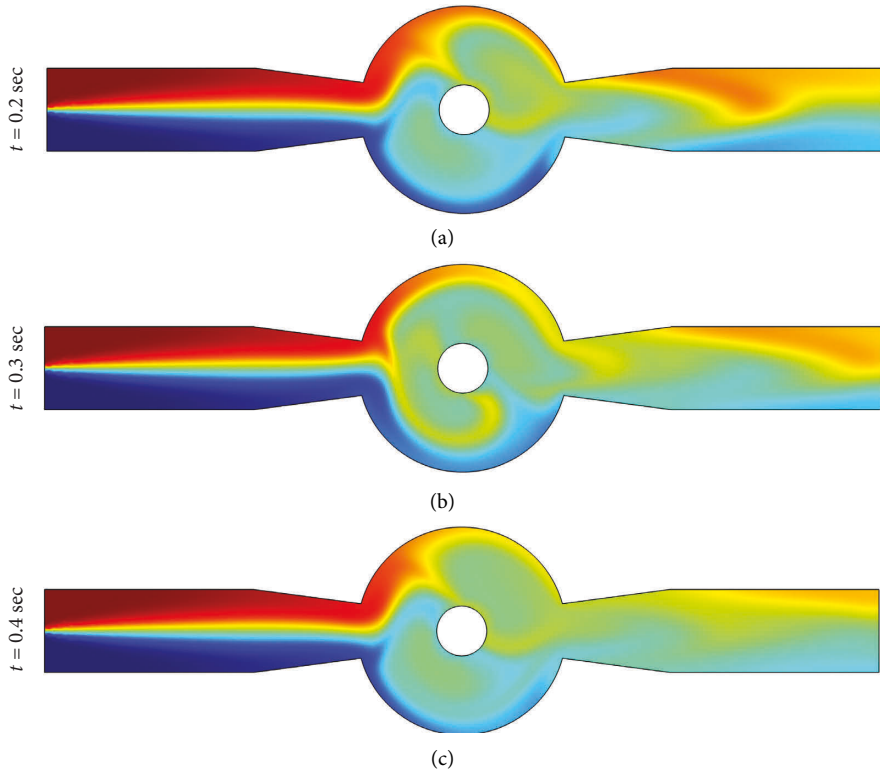

Figure 7: Concentration contour for the circular geometry at three times ($f = 5$, $u = 0.1$, and $\varphi = 0$), (a) $t = 0.2$ s; (b) $t = 0.3$ s; (c) $t = 0.4$ s.

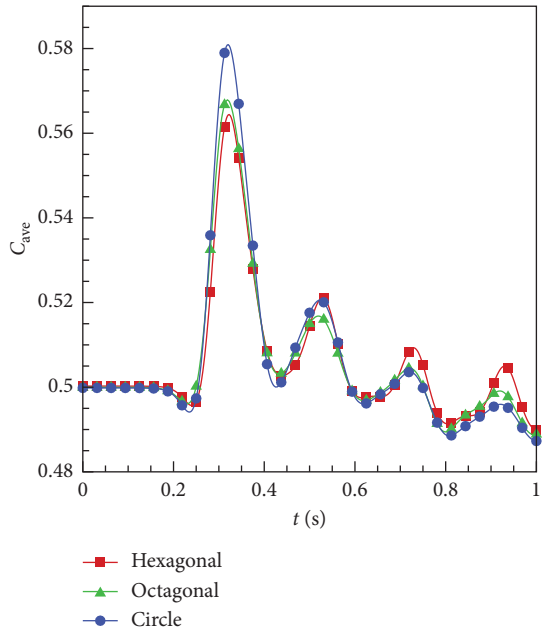

Figure 8: Average concentration variation (mol.m^{-3}) in the three geometries for $f = 5$, $u = 0.1$ mm·s^{-1}, and $\varphi = 0$.

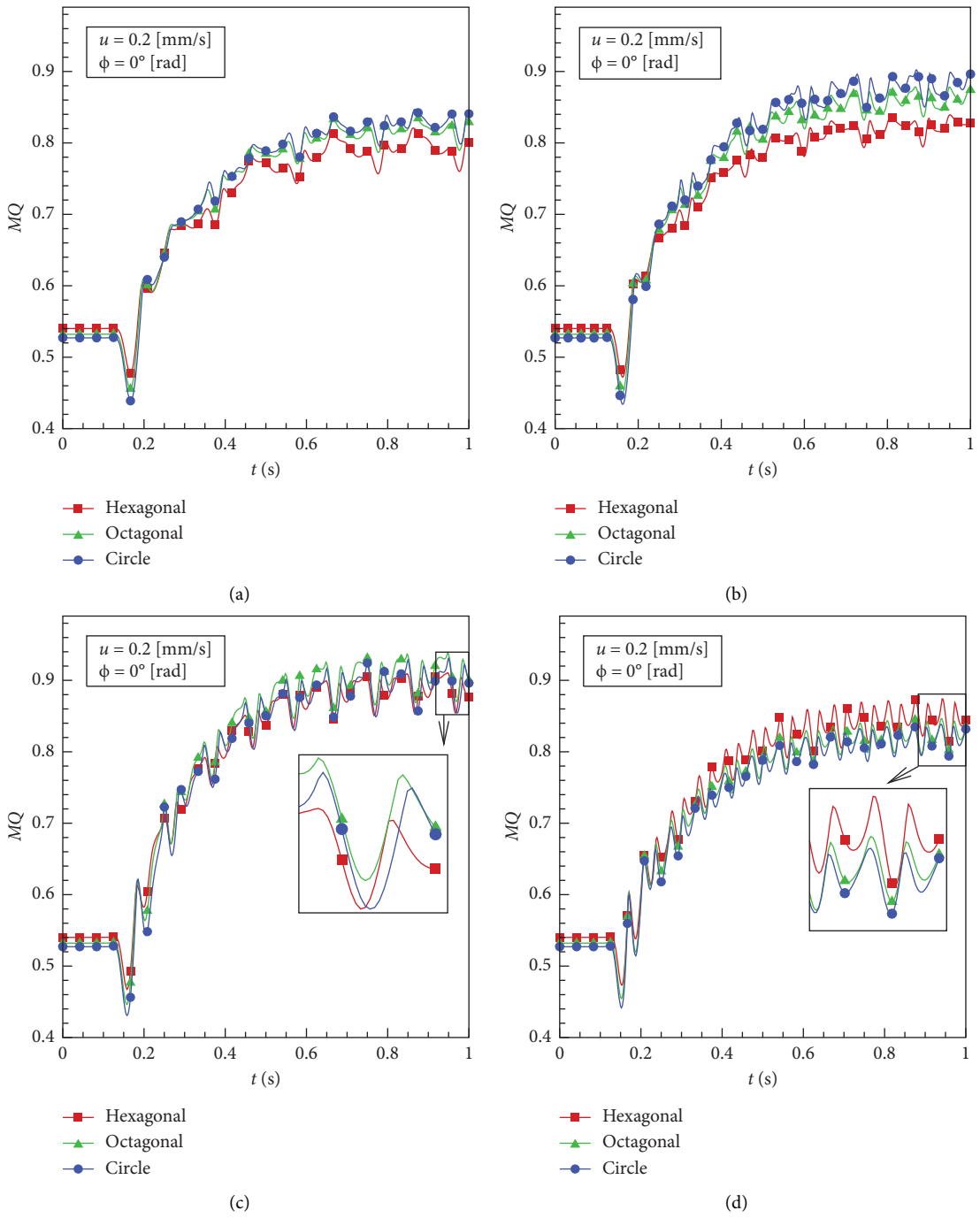

Figure 9: Mixing efficiency in three mixing chambers at $u = 0.2$ mm·s^{-1} and $\varphi = 0$ for different frequencies: (a) 5 Hz; (b) 7 Hz; (c) 10 Hz; and (d) 15 Hz.

Table 3: Mixing efficiency at $f = 15$ Hz and $\varphi = \pi$.

Fluid velocity (mm.s^{-1})	$u = 0.1$ mm/s (%)	$u = 0.15$ mm/s (%)	$u = 0.2$ mm/s (%)
Hexagonal	94.28	89.81	82.97
Octagonal	92.88	88.92	82.88
Circular	91.33	88.23	82.65

Table 4: Mixing efficiency at $t = 1$s in the three geometries at $u = 0.1\ \text{mm s}^{-1}$ and $f = 5$ Hz.

Phase difference (Rad)	$\varphi = 0$ (%)	$\varphi = \pi/2$ (%)	$\varphi = \pi$ (%)
Hexagonal	93.97	96.34	94.05
Octagonal	95.3	96.72	95.47
Circular	95.58	97.21	95.95

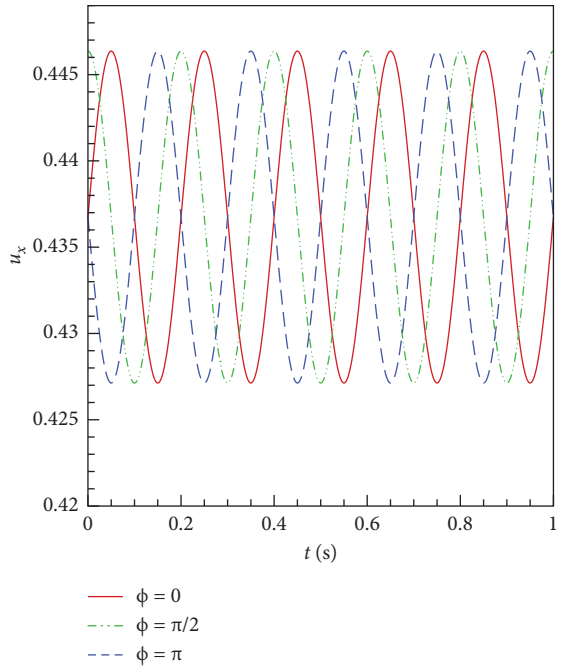

Figure 10: Velocity variations in the hexagonal inlet at $f = 5$ Hz and $u = 0.2\ \text{mm·s}^{-1}$ for three phase difference levels (0, $\pi/2$, and π).

Table 5: Mixing efficiencies at $t = 1$ s for $u = 0.1\ \text{mm·s}^{-1}$ and $\varphi = \pi/2$ at different frequencies.

Frequency (Hz)	$f = 5$ (%)	$f = 10$ (%)	$f = 15$ (%)
Hexagonal	96.34	98.16	95.91
Octagonal	96.72	97.86	95.78
Circular	97.21	97.63	95.23

where $V(V)$ is the electric potential, u_E denotes the electroosmotic velocity, E is the electric field intensity (V/m), ε shows the fluid's electric permittivity (F/m), and ε is defined as follows:

$$\varepsilon = \varepsilon_0 \varepsilon_r, \tag{3}$$

where ε_0 is the vacuum permittivity and ε_r represents the dielectric constant.

3.2. Electrical Field. Laplace's equation for obtaining scalar electric potential is expressed as follows:

$$\nabla^2 V = 0. \tag{4}$$

A time-varying sinusoidal alternating current was applied on the electrodes of the Boundaries 7 and 8, and other boundaries were isolated and expressed as follows:

$$\begin{aligned} -\sigma \nabla V.n &= 0, \\ V &= V_0 \sin(\omega t + \varphi), \\ \omega &= \frac{2\pi}{f}, \end{aligned} \tag{5}$$

where σ denotes the permittivity (S/m), ω represents angular frequency, t is the time based on seconds, V is the differential potential of sinusoidal wave, f is the frequency based on Hertz, and φ is the phase difference. Table 1 indicates the parameters utilized in this simulation.

3.3. Concentration Field. While being mixed, the fluid is a function of advection-diffusion equation expressed as follows:

$$\nabla \cdot j_i = 0, \tag{6}$$

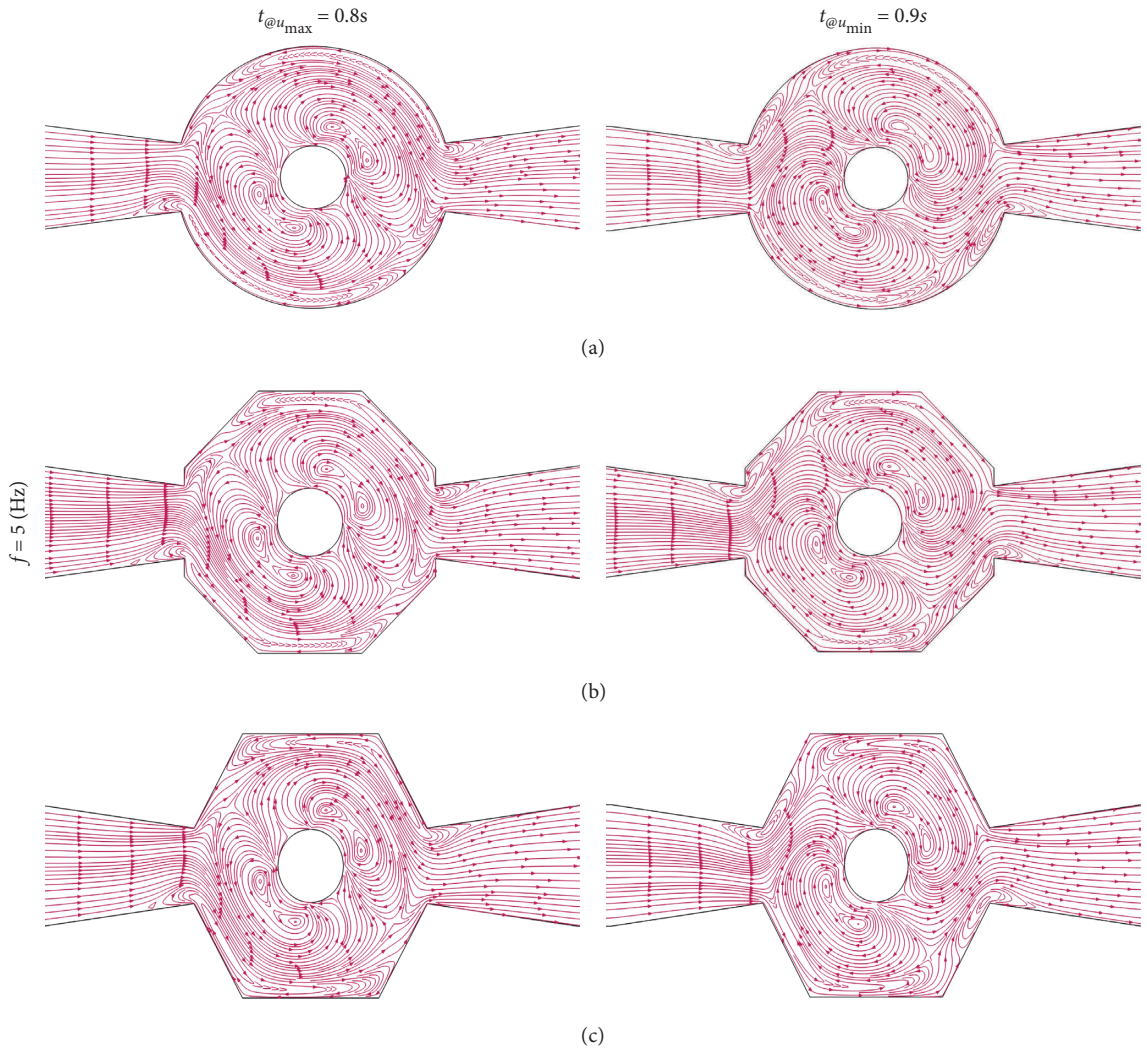

Figure 11: Streamlines in (a) circular, (b) octagonal, and (c) hexagonal mixing chambers for the maximum (left) and minimum (right) velocities in the final cycle at $f = 5$ Hz ($u = 0.1$ mm·s^{-1}, $\varphi = \pi/2$).

where j_i is the flux of the species i and j is the mass flux defined as follows:

$$j_i = -D_i \nabla C_i + uC_i. \tag{7}$$

Moreover, to express the flux of species, the intended system can be explicated using the following equation:

$$\frac{\partial c}{\partial t}(V \cdot \nabla)C = D\nabla^2 C, \tag{8}$$

where c denotes the concentration of species (in mol/m^3), D denotes the diffusion coefficient (in m^2/s), and U is the flow velocity. Boundary conditions in concentration modeling are established as equal to 0 at the lower half of the inlet wall and equal to 1 at the upper half.

3.4. Evaluation Criteria for Mixing. Mixing quality, as defined by Eq. (5), is used to show how well the micromixer is able to mix the species.

$$\mathrm{MQ} = 1 - \frac{\int_0^L |c - c_m| \mathrm{d}y}{\int_0^L |c_0 - c_m| \mathrm{d}y}, \tag{9}$$

where MQ is the mixing quality, C_m is the concentration of the species in a perfect mix (0.5), C_0 is the concentration at the micromixer inlet, and C is the concentration distribution at an arbitrary downstream cross-section. The outlet size is denoted as L to calculate the mixing quality at the micromixer outlet.

4. Mesh and Validation

The solution's independence of the number of elements and six levels of solution with different meshing conditions as listed in Table 2 were carried out. It is evident from Figure 2 that increasing the number of elements from that in the fourth solution to the level of the fifth solution makes little change in terms of C_{ave}, and adding even more elements, as in the sixth solution, results in negligible difference.

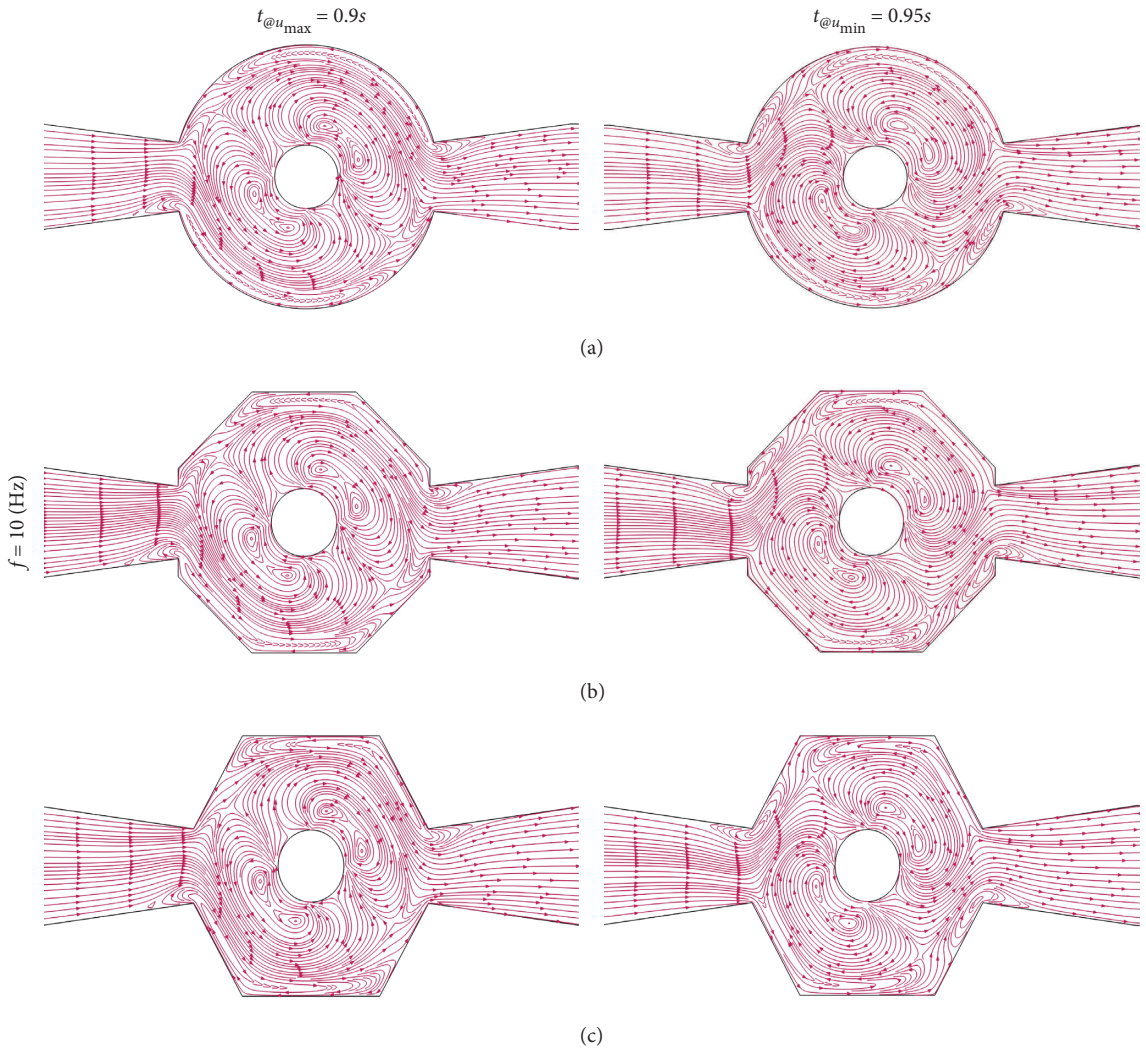

FIGURE 12: Streamlines in (a) circular, (b) octagonal, and (c) hexagonal mixing chambers for the maximum (left) and minimum (right) velocities in the final cycle at $f = 10$ Hz ($u = 0.1$ mm·s^{-1}, $\varphi = \pi/2$).

Accordingly, based on the resulting C_{ave} for each level of meshing, the fifth solution (obtained with 18,076 elements) was adopted as the optimal meshing, guaranteeing the solution's grid independence.

Figure 3 depicts the mesh used in the fifth solution of Table 2 for the three geometries.

A case from the literature was also considered to validate and evaluate the accuracy. Cheng et al. [22] created a numerical simulation of electroosmotic mixing with three periodic potential functions, namely, sinusoidal, square, and zigzag, in a T-shaped micromixer. They studied a micromixer with two inlets for two fluids of different concentrations (0 and 0.1 mol·m^{-3}) running at the same velocity (0.002 m·s^{-1}). Further, four electrodes were installed on the outlet channel walls. Figure 4(a) depicts the concentration contours for the sinusoidal potential for comparison with the reports of Cheng et al. at 0.02/3 s and 100 Hz (Figure 4(b)). Further, Figure 5 plots concentration changes against time under sinusoidal voltage at 400 Hz for a more accurate investigation. Figures 4 and 5 are suggestive of the consistency of the present work's results with the reports of Cheng et al. [22], which can be seen in terms of the trends in the diagrams, as well as the data.

5. Results and Discussion

5.1. The Effect of Geometry on the Mixing Quality in Various Frequencies. Figure 6shows the mixing quality of the three mixing chambers at 0.1 mm·s^{-1}, 0 rad phase difference, and 5, 7, 10, and 15 Hz frequencies. As evident from Figure 6(a), at 5 Hz, the micromixer with a circular mixing chamber offers the highest mixing efficiency, and reducing the number of sides at this frequency has an adverse effect undermined mixing. Figure 6(b), plotted at 7 Hz, shows a change in behavior in terms of mixing efficiency, and this frequency range can be considered a turning point for the effect of the number of sides on the mixing efficiency. Figures 6(c) and 6(d) indicate a decline in mixing efficiency at higher frequencies as the sides are increased. The outcome can be attributed to the increased vortex formation in geometries with fewer sides and angles, which

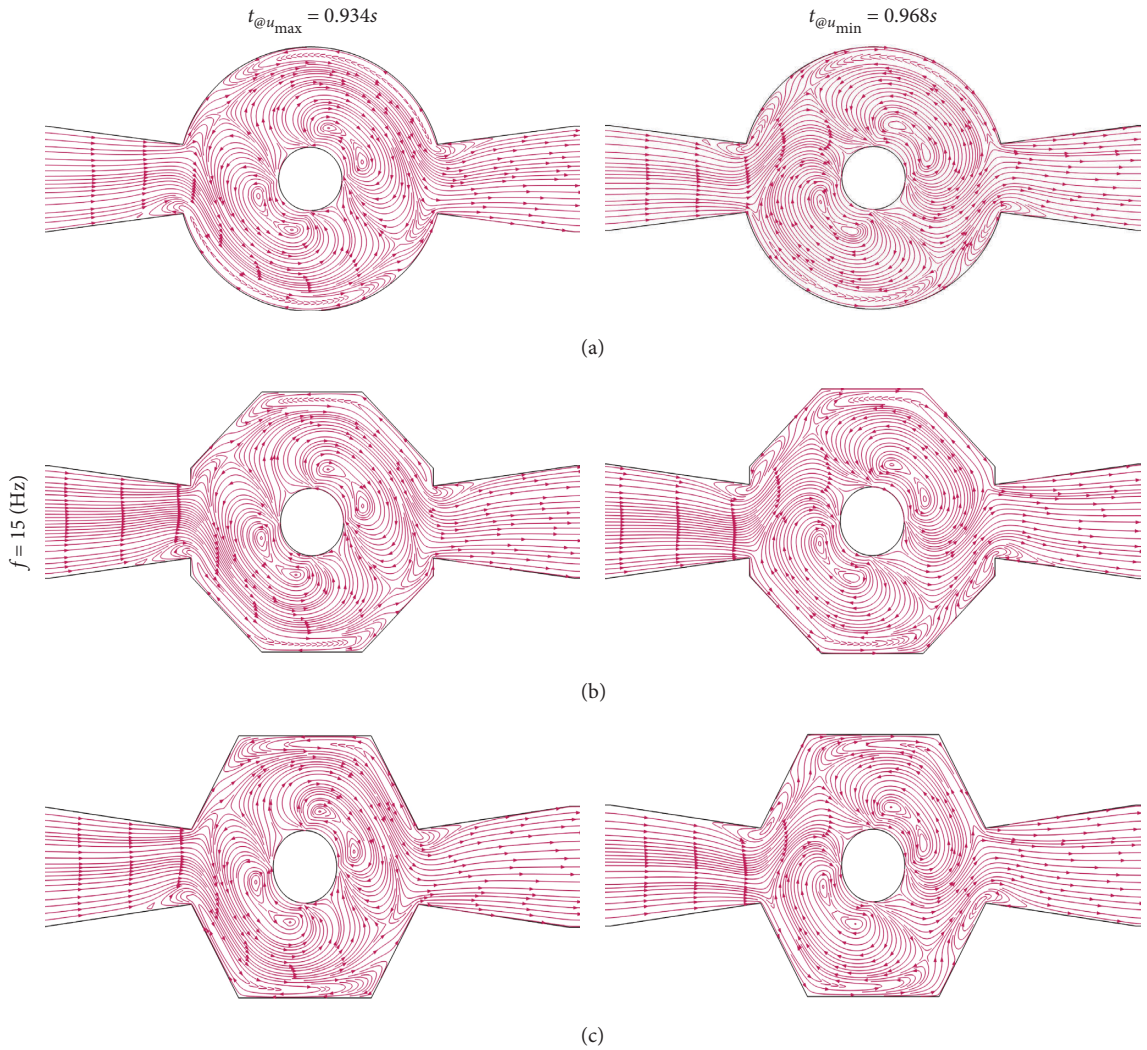

FIGURE 13: Streamlines in (a) circular, (b) octagonal, and (c) hexagonal mixing chambers for the maximum (left) and minimum (right) velocities in the final cycle at $f = 15$ Hz ($u = 0.1$ mm·s^{-1}, $\varphi = \pi/2$).

promotes fluid mixing. Further, according to Figure 6(d), at 15 Hz, the highest mixing quality corresponds to the hexagonal chamber followed by octagonal and circular geometries.

According to Figures 6(a)-6(d), a sudden drop in mixing efficiency is found at 0.3 s in all geometries and frequencies. It is evident from the mixing contours plotted for the circular geometry at different times (Figure 7) that the drop in mixing efficiency can be attributed to the imperfect mixing of the two fluids in the 0.2-0.4 s interval, when a substantial volume of the high-concentration input fluid reaches the micromixer's outlet boundary, resulting in a sudden hike in the concentration. According to Eq. (5), this move away from the 0.5 concentration (perfect mix) reduces the mixing efficiency of the two fluids. It should be noted that with increasing frequency, the amount of this sudden drop has decreased, which is due to the formation of more vortices at a higher frequency, which causes higher mixing of the two fluids.

Figure 8 depicts the average concentration at each micromixer outlet of the three mixing chambers at 0.1 mm·s^{-1} and 5 Hz with 0 rad phase difference. Evidently, the highest average concentration was achieved in the 0.2-0.4 s interval, showing a decline in the mixing efficiency. Further, Figure 7(c) shows that the fluid reaching the micromixer outlet at the specified intervals has a higher concentration and, accordingly, a lower mixing efficiency.

According to Figure 9, the direct effects of the chamber geometry on the mixing quality when increasing the electric current frequency will be observed at a higher frequency range when the inlet velocity is raised from 0.1 to 0.2 mm·s^{-1}.

As evident from Figures 6 and 9, the simulations show that, for both 0.1 and 0.2 mm·s^{-1} inlet velocities, the circular, octagonal, and hexahedral geometries produced the highest to lowest mixing quality at 5 Hz, while at 15 Hz, the hexagonal offered the highest efficiency, followed by the octagonal and the circular. It must be noted that the geometry effects of the mixing chamber on the mixing quality are manifested in a transition range from 5 to 15 Hz. That is to say, at 0.1 mm·s^{-1}, the octagonal, circular, and hexagonal geometries produce the highest to the lowest mixing quality

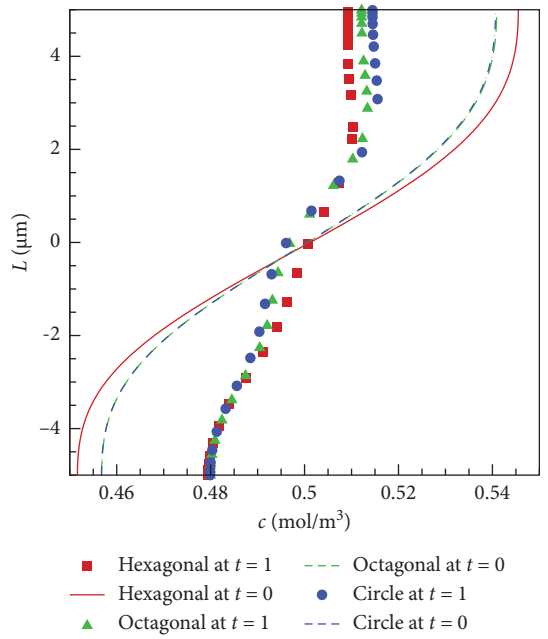

Figure 14: Variation of concentration based on the changes in length in 3 different mixing chambers when $u = 0.1\,[mm/s]$, $\varphi = \pi/2$ and $f = 10\,[Hz]$ at different times.

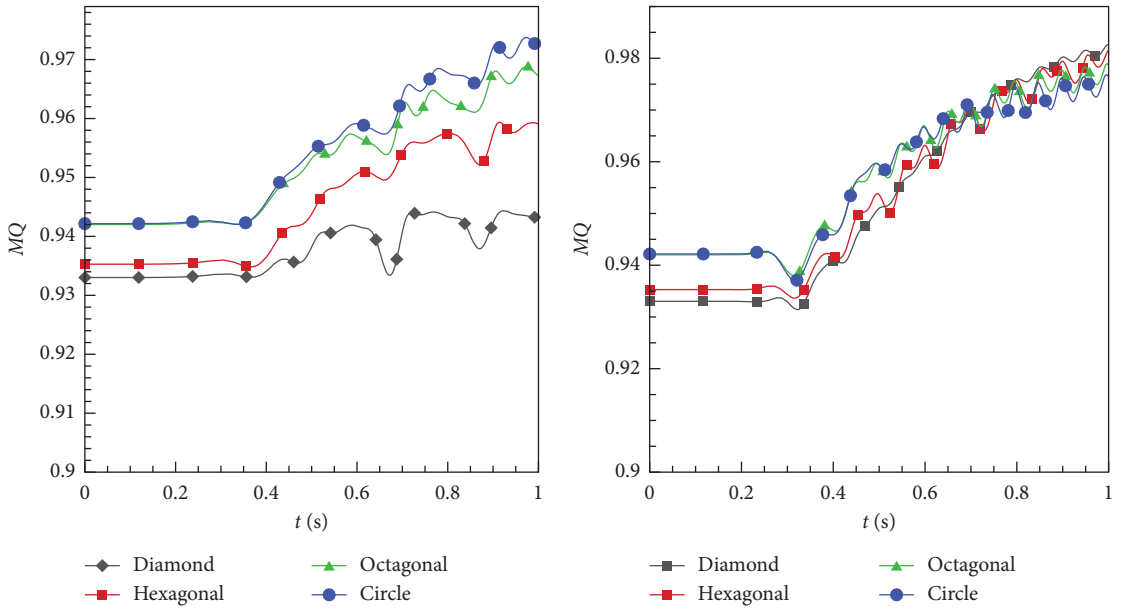

Figure 15: Variation of mixing quality in the simulation time in different mixing chambers when $u = .01\,[mm/s]$, $\varphi = \pi/2$, $f = 5\,[Hz]$ (left) and $u = .01\,[mm/s]$, $\varphi = \pi/2$, $f = 10\,[Hz]$ (right).

in the 5-7 Hz range. By raising the inlet velocity to 0.2 mm·s^{-1}, the same observation can be made in the 7-10 Hz range, showing the effect of mixing chamber geometry on the mixing quality at different inlet velocities and frequencies. It is safe to say that by raising the frequency from 5 to 15 Hz, a higher mixing quality can be achieved with a mixing chamber with fewer sides. Another noteworthy point is that by comparing Figures 6 and 9, it can be seen that the sudden drop in mixing efficiency occurs faster and is in the time range of 0.1 to 0.2, and this issue was completely predictable. For example, the speed of the fluid has increased and it causes a large volume of the input fluid with a higher concentration to reach the outlet boundary of the micromixer faster. Similarly, with increasing frequency, more vortices are created and as a result, the amount of this sudden drop decreases.

5.2. Changes of Mixing Efficiency under Different Parameters. Table 3 lists the mixing efficiencies for the output fluid in the three micromixers at $t = 1$ s and 15 Hz for different velocities

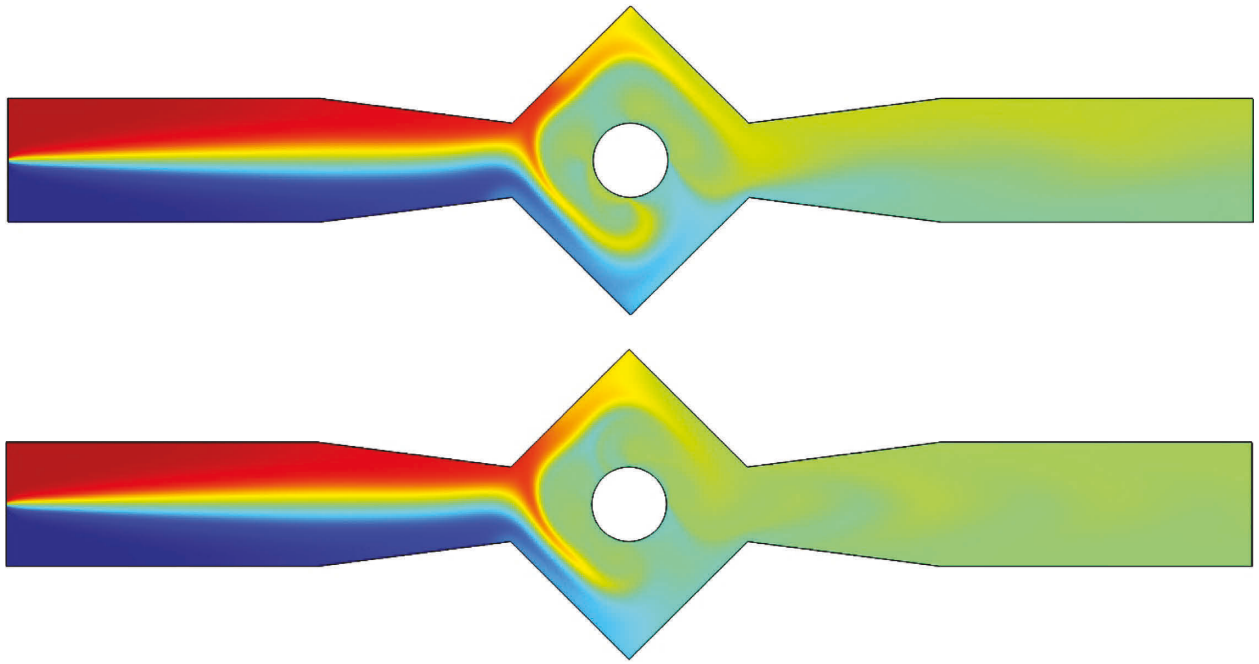

Figure 16: Contours of the changes in the concentration in the diamond-shaped mixing chamber when $u = 0.1\,[mm/s]$, $\varphi = \pi/2$, $f = 5\,[Hz]$ (up) and $u = .01\,[mm/s]$, $\varphi = \pi/2$, $f = 10\,[Hz]$ (down).

(namely, 0.1, 0.15, and 0.2 mm·s^{-1}) for a phase difference of π. From the data in Table 3, it can be concluded that by increasing the speed of the fluid at the entrance of the micromixer, the time the fluid remains in the mixing chamber decreases and it is exposed to the electric field from the electrodes embedded in the mixing chamber for a shorter period of time. By reducing this time, less eddies are formed in the fluid and two fluids with different concentrations are mixed with each other to a lesser extent, and therefore the mixing effect decreases with increasing speed.

It is evident from the results in Table 4 that the highest mixing level in all chambers is achieved with the $\pi/2$ phase difference, which maximizes $\sin(\omega t)$ for the most number of times. Figure 10 shows the axial velocity at the middle point of the hexagonal chamber inlet in the three frequencies. It is also evident that the fluid reaches maximum velocity more in this case (6 times) than in the other two configurations (5 times), forming more vortices, which improves mixing.

Table 5 presents the mixing efficiency of the three studied geometries at $t = 1$ s for $u = 0.1$ and $\varphi = \pi/2$. With knowledge of the fact that the highest mixing quality is achieved with a velocity of 0.1 mm·s^{-1} and a phase difference of $\pi/2$, Table 5 presents the efficiency at different frequencies for this velocity and phase difference.

Based on the data in Table 5, the highest mixing quality is achieved in all chambers at 10 Hz. In view of the results, based on the Helmholtz–Skolimowski equation and given the effect of electric current on the fluid motion on the one hand, and the effects of current frequency on vortex formation on the other, two concurrent effects can be said to be in force. Increasing the frequency hinders mixing due to the increased fluid velocity and reduced fluid retention time in the mixing chamber, but it also promotes vorticity and changes the flow pattern, which improves mixing. The two simultaneous effects make 10 Hz the optimal frequency for mixing.

5.3. Changes of Streamlines. Figures 11-13 depict the fluid streamlines in the mixing chamber at $u = 0.1$ mm·s^{-1}, $\varphi = \pi/2$, and different frequencies (5, 10, and 15 Hz). Based on the mixing quality and mixing improvement by the end of the studied interval, the streamline graphs indicate two periods. These periods correspond to the highest and lowest velocities along the x-direction in the final cycle at each frequency and are calculated, according to $T = 1/f$, at 0.8 and 0.9 s for 5 Hz, 0.9 and 0.95 s for 10 Hz, and 0.934 and 0.968 s for 15 Hz. The figures show the effects of frequency on the flow pattern and vertex formation in the chambers, verifying the influence of the chamber sides' geometry on mixing.

Figure 14 shows mixing at the channel outlet for the initial and the last time periods of the most optimum mixing state that occurs at a velocity of 0.1, a frequency of 10 Hz, and a phase difference of $\pi/2$, for all three mixing chambers; as can be seen, at the end of the solving time, fluid concentration in the outlet of the hexagonal micromixer is better than that of the other two mixing chambers, being almost fully mixed. The reason for this is the creation of more vortices and changes in the speed and direction of fluid movement, which, as a result, increases the time the fluid remains in the mixing chamber.

To verify the results, a rhombic mixing chamber, surrounded by a circle, with all boundary conditions of previous micromixers was simulated. Figures 15 and 16 show the mixing percentage and the concentration contour,

respectively. It was found that in micromixers with symmetric chambers and a specific velocity and phase difference, higher mixing rate is achieved by using a mixing chamber with a higher number of sides and a bigger area at lower frequencies and a mixing chamber with lesser number of sides and a smaller area at higher frequencies.

6. Conclusion

Rapid technological advancement in the field of micromixing urges further investigation due to extensive applications in engineering, medicine, and biology. Notable objectives regarding micromixers include achieving the highest mixing efficiency in the shortest time possible. In this light, the present study investigated three two-dimensional electroosmotic micromixers with circular, hexagonal, and octagonal mixing chambers through a coupled solution of the flow, concentration, and electric fields by the finite-element tool, COMSOL Multiphysics 5.4. The aim was to study and optimize the simultaneous and mutual effects of inlet velocity, frequency, phase difference, and the mixing-chamber geometry on the mixing efficiency of the micromixer output. The most notable findings of the simulations can be summarized as follows:

(i) Increasing the electric current frequency amplifies the chamber geometry effects. That is, mixing is improved at higher frequencies in geometries with fewer sides, and these effects are observed at a higher frequency range when the inlet velocity is increased. For example, with an inlet velocity of 0.1 mm·s^{-1}, the octagonal and hexagonal offered the highest mixing quality at 7 and 10 Hz. However, raising the inlet velocity to 0.2 mm·s^{-1} pushed the frequencies to 10 and 15 Hz, respectively.

(ii) Increasing the inlet velocity reduced the mixing efficiency in all geometries—due to the lower retention time in the mixing chamber—while increasing the slope of mixing efficiency variations against time, as well as the number and amplitude of the variations due to the increased vorticity.

(iii) The highest mixing quality was achieved with an inlet velocity of 0.1 mm·s^{-1}, a frequency of 10 Hz, and a phase difference of $\pi/2$ in all geometries.

(iv) The overall highest mixing efficiency (98.16%) was achieved with the hexagonal mixing chamber under optimal conditions.

Abbreviations

Parameters

c: Concentration of fluids (mol/m^3)
c_0: Initial concentration of diffusing species (mol/m^3)
c_m: Concentration of fully mixed state (mol/m^3)
D: Diffusion coefficient of the solution (m^2/s)
u_E: Electro-osmotic velocity (m/s)
E: Electric field intensity (V/m)
f: Frequency applied to the electrodes (Hz)
F: Body force (N/m^3)
J: Diffusive flux (mol/m^{2}s^{-1})
L: The width of inlet and outlet
MQ: Mixing quality
n: Normal vector
p: Pressure (Pa)
t: Time (s)
T: Period (s)
u: Velocity vector (m/s)
U_0: Mean inflow velocity (mm/s)
V_0: Amplitude of voltage applied to the electrodes (V)
V: Electric potential (V)

Greek symbols

ε: Electric permittivity of fluid (F/m)
ϵ_r: Relative permittivity of the fluid (F/m)
ϵ_0: Permittivity of free space (F/m)
ξ: Zeta potential (V)
μ: Dynamic viscosity (Pa.s)
ρ: Density (kg/m^3)
σ: Conductivity of ionic solution (S/m)
φ: Phase difference (rad)
ω: Angular frequency

Subscripts

Ave: Average
E: Electro-osmosis
x: x-direction
y: y direction.

Data Availability

All data used to support the findings of this study are included within the article.

Conflicts of Interest

The authors declare that they have no conflicts of interest.

References

[1] M. Alipanah and A. Ramiar, "High efficiency micromixing technique using periodic induced charge electroosmotic flow: a numerical study," *Colloids and Surfaces A: Physicochemical and Engineering Aspects*, vol. 524, pp. 53–65, 2017.

[2] S. Ebrahimi, A. Hasanzadeh-Barforoushi, A. Nejat, and F. Kowsary, "Numerical study of mixing and heat transfer in mixed electroosmotic/pressure driven flow through T-shaped microchannels," *International Journal of Heat and Mass Transfer*, vol. 75, pp. 565–580, 2014.

[3] W. Hong, H. Shi, Z. Huang et al., "Design and simulation of a passive micromixer with gourd-shaped channel," *Journal of Nanoscience and Nanotechnology*, vol. 19, no. 1, pp. 206–212, 2019.

[4] Z. Wu and X. Chen, "Numerical simulation of a novel microfluidic electroosmotic micromixer with Cantor fractal structure," *Microsystem Technologies*, vol. 25, no. 8, pp. 3157–3164, 2019.

[5] D. Nouri, A. Zabihi-Hesari, and M. Passandideh-Fard, "Rapid mixing in micromixers using magnetic field," *Sensors and Actuators A: Physical*, vol. 255, pp. 79–86, 2017.

[6] B. Mondal, S. K. Mehta, S. Pati, and P. K. Patowari, "Numerical analysis of electroosmotic mixing in a heterogeneous charged micromixer with obstacles," *Chemical Engineering*

and Processing-Process Intensification, vol. 168, Article ID 108585, 2021.

[7] A. Ahmadian Yazdi, A. Sadeghi, and M. H. Saidi, "Electrokinetic mixing at high zeta potentials: ionic size effects on cross stream diffusion," *Journal of Colloid and Interface Science*, vol. 442, pp. 8–14, 2015.

[8] S. Zhang and X. Chen, "A novel passive micromixer based on Koch fractal principle," *Journal of the Brazilian Society of Mechanical Sciences and Engineering*, vol. 40, no. 10, pp. 487–489, 2018.

[9] X. Tian, Y. Yuan, S. Fan, B. Zhou, H. Liao, and H. Yuan, "Numerical simulation analysis of electroosmotic micromixing in Y-shaped micro-channel," in *Recent Developments in Intelligent Computing, Communication and Devices*-Springer, Berlin, Germany, 2019.

[10] Y. Deng, T. Zhou, Z. Liu, Y. Wu, S. Qian, and J. G. Korvink, "Topology optimization of electrode patterns for electroosmotic micromixer," *International Journal of Heat and Mass Transfer*, vol. 126, pp. 1299–1315, 2018.

[11] M. Nazari, P.-Y. A. Chuang, J. Abolfazli Esfahani, and S. Rashidi, "A comprehensive geometrical study on an induced-charge electrokinetic micromixer equipped with electrically conductive plates," *International Journal of Heat and Mass Transfer*, vol. 146, Article ID 118892, 2020.

[12] B. Keshavarzian, M. Shamshiri, M. Charmiyan, and A. Moaveni, "Optimization of an active electrokinetic micromixer based on the number and arrangement of microelectrodes," *Journal of Applied Fluid Mechanics*, vol. 11, no. 6, pp. 1531–1541, 2018.

[13] K.-R. Huang, Z.-H. Hong, and J.-S. Chang, "Microfluidic mixing on application of traveling wave electroosmosis," *European Journal of Mechanics—B: Fluids*, vol. 48, pp. 153–164, 2014.

[14] J.-L. Chen, W.-H. Shih, and W.-H. Hsieh, "AC electro-osmotic micromixer using a face-to-face, asymmetric pair of planar electrodes," *Sensors and Actuators B: Chemical*, vol. 188, pp. 11–21, 2013.

[15] A. Shamloo, M. Mirzakhanloo, and M. R. Dabirzadeh, "Numerical simulation for efficient mixing of Newtonian and non-Newtonian fluids in an electro-osmotic micro-mixer," *Chemical Engineering and Processing-Process Intensification*, vol. 107, pp. 11–20, 2016.

[16] K. Matsubara and T. Narumi, "Microfluidic mixing using unsteady electroosmotic vortices produced by a staggered array of electrodes," *Chemical Engineering Journal*, vol. 288, pp. 638–647, 2016.

[17] M. Ghandchi, "AC electrothermal actuation mechanism for on-chip mixing of high ionic strength fluids," *Microsystem Technologies*, vol. 23, 2017.

[18] M. Nazari, S. Rashidi, and J. A. Esfahani, "Effects of flexibility of conductive plate on efficiency of an induced-charge electrokinetic micro-mixer under constant and time-varying electric fields-a comprehensive parametric study," *Chemical Engineering Science*, vol. 212, Article ID 115335, 2020.

[19] S. Najjaran, S. Rashidi, and M. S. Valipour, "A new design of induced-charge electrokinetic micromixer with corrugated walls and conductive plate installation," *International Communications in Heat and Mass Transfer*, vol. 114, Article ID 104564, 2020.

[20] A. Qaderi, J. Jamaati, and M. Bahiraei, "CFD simulation of combined electroosmotic-pressure driven micro-mixing in a microchannel equipped with triangular hurdle and zeta-potential heterogeneity," *Chemical Engineering Science*, vol. 199, pp. 463–477, 2019.

[21] A. Shamloo, M. Madadelahi, and S. Abdorahimzadeh, "Three-dimensional numerical simulation of a novel electroosmotic micromixer," *Chemical Engineering and Processing: Process Intensification*, vol. 119, pp. 25–33, 2017.

[22] Y. Cheng, Y. Jiang, and W. Wang, "Numerical simulation for electro-osmotic mixing under three types of periodic potentials in a T-shaped micro-mixer," *Chemical Engineering and Processing-Process Intensification*, vol. 127, pp. 93–102, 2018.

[23] H. Song and D. J. Bennett, "Numerical study of enhancing the mixing effect in microchannels via transverse electroosmotic flow by placing electrodes on top and bottom of the channel," *Microsystem Technologies*, vol. 17, no. 9, pp. 1427–1437, 2011.

[24] H. M. Park and T. W. Kim, "Extension of the Helmholtz-Smoluchowski velocity to the hydrophobic microchannels with velocity slip," *Lab on a Chip*, vol. 9, no. 2, pp. 291–296, 2009.